Inversion-Protected Higher-Order Topological Superconductivity in Monolayer WTe_2

Yi-Ting Hsu,* William S. Cole, Rui-Xing Zhang, and Jay D. Sau
Condensed Matter Theory Center and Joint Quantum Institute, University of Maryland, College Park, Maryland 20742, USA

(Received 21 July 2019; accepted 6 August 2020; published 24 August 2020)

Monolayer WTe_2, a centrosymmetric transition metal dichacogenide, has recently been established as a quantum spin Hall insulator and found superconducting upon gating. Here we study the pairing symmetry and topological nature of superconducting WTe_2 with a microscopic model at mean-field level. Surprisingly, we find that the spin-triplet phases in our phase diagram all host Majorana modes localized on two opposite corners. Even when the conventional pairing is favored, we find that an intermediate in-plane magnetic field exceeding the Pauli limit stabilizes an unconventional equal-spin pairing aligning with the field, which also hosts Majorana corner modes. Motivated by our findings, we obtain a recipe for two-dimensional superconductors featuring "higher-order topology" from the boundary perspective. Generally, a superconducting inversion-symmetric quantum spin Hall material whose normal-state Fermi surface is away from high-symmetry points, such as gated monolayer WTe_2, hosts Majorana corner modes if the superconductivity is parity-odd. We further point out that this higher-order phase is an inversion-protected topological crystalline superconductor and study the bulk-boundary correspondence. Finally, we discuss possible experiments for probing the Majorana corner modes. Our findings suggest superconducting monolayer WTe_2 is a playground for higher-order topological superconductivity and possibly the first material realization for inversion-protected Majorana corner modes *without* utilizing proximity effect.

DOI: 10.1103/PhysRevLett.125.097001

Introduction.—Extensive experimental and theoretical effort has been devoted to transition metal dichalcogenides, a family of materials with the chemical formula MX_2 (M = transition metal, X = S, Se, Te) known to host a rich variety of intriguing ground states such as topological insulators and semimetals [1–6], charge density waves [7–13], and various types of possibly unconventional superconductivity [13–21]. Moreover, tuning among these phases is possible by widely accessible experimental knobs—for example, changing the thickness, pressure [10,22–25], electrostatic gating [13,16,26], and recently even the twist angle between monolayers [27,28]. Recently, a centrosymmetric member of the transition metal dichalcogenides family, monolayer WTe_2, has been established [1–4,29,30] as a quantum spin Hall (QSH) insulator [31,32]. Remarkably, in this same material, superconductivity at temperatures around 1 K was soon after reported under tunable electrostatic gating [20,21]. We are thus motivated to understand the nature of this superconductivity given the prevailing expectation that inducing superconductivity in already topological materials is a promising route for achieving topological superconductors.

Theoretically, a known necessary condition for two-dimensional (2D) time-reversal topological superconductors requires negative pairing potentials on an odd number of Fermi surfaces that enclose time-reversal invariant momenta (TRIMs) [33,34]. The presence of the inversion symmetry, however, enforces twofold degeneracy of the Fermi surfaces and thus sets up a "no-go" theorem that precludes such superconductors from being topological. Nonetheless, recent developments suggest that inversion can unexpectedly enrich the topological structure of a system [35–37] and enable new topological crystalline superconductors (TCsc) that are completely beyond the previous paradigm [33,34]. In particular, there exists a type of inversion-protected TCsc in dimension d that has no Majorana boundary modes in $d-1$ dimension yet is still topologically distinct from a trivial superconductor [36,37]. This suggests the possibility that such an inversion-protected TCsc belongs to the so-called "higher order topological phases" [38–48] and may host Majorana boundary modes in $d-2$ or lower dimensions.

Here, we propose a surprisingly simple recipe for this exotic inversion-protected TCsc: (1) the normal state is an inversion-symmetric QSH material with Fermi pockets away from TRIMs, and (2) the superconductivity is parity-odd. Given that gated monolayer WTe_2 readily satisfies criteria (1), unconventional superconductivity with odd parity becomes the last piece of the puzzle for an inversion-protected TCsc that could host exotic Majorana corner modes.

In fact, in WTe_2 there is ample reason to suspect that electron correlations might be strong, and odd-parity superconductivity is therefore plausible. First is the fact that the reported superconductivity [20,21] occurs at a low carrier density, while *ab initio* calculations do not reproduce the low-energy normal state band structure found by angle-resolved photoemission spectroscopy

(ARPES) [2] and STM [2] studies unless one goes beyond the generalized-gradient approximation [1,2,49]. Moreover, the reported in-plane upper critical field $H_{c2}^{\parallel}$ is 2.5 to 4.5 times higher than the Pauli limit H_p [20,21]. While an $H_{c2}^{\parallel}$ higher than the Bardeen-Cooper-Schrieffer theory prediction in centrosymmetric materials can occur when the normal state has a high spin-orbit scattering rate [50] or when the g factor deviates from 2 [20], another possible origin is a spin-triplet (and thus odd-parity) paired state with spin aligning in the field direction.

In this work, we report the pairing symmetry and topological nature of the newly discovered superconductivity in gated monolayer WTe_2. First, we solve the linearized gap equations to obtain a superconducting phase diagram in terms of microscopic interactions. By investigating the boundary modes in different phases, we find Majorana corner modes in odd-parity phases and, surprisingly, also in the field-induced equal-spin phase emerging upon the suppression of conventional pairings. Then, we obtain a general recipe from the boundary perspective for achieving such 2D superconductivity with corner Majoranas. Finally, we point out that such higher-order phase is an inversion-protected topological crystalline superconductor that can be characterized by a bulk invariant we propose, and we address the bulk-boundary correspondence. Our recipe provides a new route toward materializing a novel topological phase of matter, as well as realizing Majorana zero modes, which is the first step for topological quantum computation.

Model.—Monolayer WTe_2 is stable in the $1T'$ structure, which is a buckled honeycomb lattice that is distorted into a rectangular lattice consisting of in-plane and buckled zigzag chains of W and Te atoms, respectively [see Fig. 1(a)].

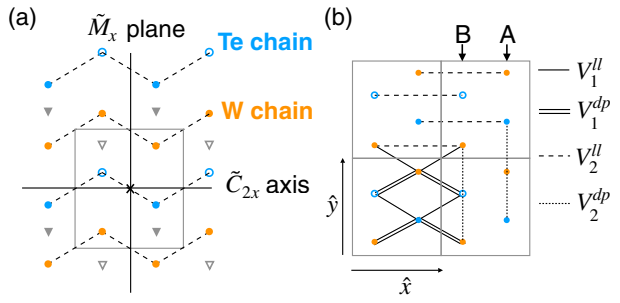

FIG. 1. Schematics for (a) the top view of the lattice of $1T'$-WTe_2, and (b) the microscopic interactions considered in Eq. (2). In (a), the filled orange circles represent the W atoms, which locate on the $z = 0$ plane. The filled and hollow blue circles (gray triangles) represent the Te atoms above and below the $z = 0$ plane, which are (are not) associated with the Wannier orbital centers in the low-energy tight-binding description. The gray rectangle indicates a unit cell, the horizontal and vertical black lines show the screw-rotation axis and the glide-mirror plane, respectively, and the black cross marks the inversion center. In (b), we omit the Te atoms (gray triangles) that do not contribute to Wannier orbitals.

This lattice is nonsymmorphic, with a twofold screw rotation C_{2x} and a glide-mirror symmetry M_x [51], each with a half-unit-cell translation along the chain direction $\hat{x}$. The lattice also has inversion symmetry I_0, resulting from the product of the two symmetries.

To study the dominant pairing channels in gated monolayer WTe_2, we start from a minimal tight-binding model previously obtained by other authors from a low-energy fit to *ab initio* calculations [52–54]. The Hamiltonian is written in a basis of spin s and four Wannier orbitals. These Wannier orbitals are labeled by the sublattice $\sigma = A$, B they are on and by whether they transform as $d_{x^2-y^2}$ or p_x orbitals ($l = d$, p). The $l = d$, p orbitals are derived from W and Te atoms, respectively. Each degree of freedom is denoted by the corresponding Pauli matrices: $\hat{s}$, $\hat{\sigma}$, and $\hat{l}$, respectively. The full normal-state Hamiltonian is

$$H_0(\boldsymbol{k}) = \hat{s}_0 \otimes [\hat{h}_0(\boldsymbol{k}) - \mu] + V_{\mathrm{soc}} \hat{s}_z \hat{\sigma}_z \hat{l}_y. \tag{1}$$

Here, the s_z-preserving intrinsic spin-orbit coupling V_{soc} [53] is the lowest order term in $\boldsymbol{k}$ that obeys time-reversal, screw-rotation, and glide-mirror symmetries, while the spin-degenerate part $\hat{h}_0(\boldsymbol{k})$ [52,53] is a 4×4 matrix in the basis of $\hat{\sigma} \otimes \hat{l}$ [Supplemental Material (SM) [56], Sec. I]. As a zeroth-order approximation to the gating effects, we set the overall chemical potential $\mu = 0.5$. The

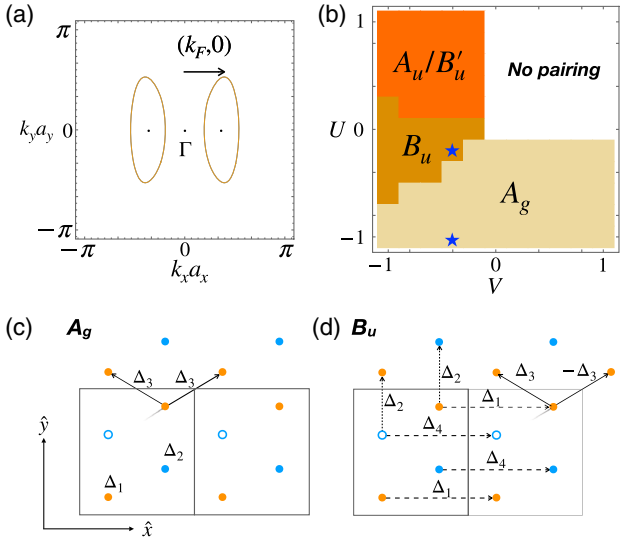

FIG. 2. (a) The two Fermi pockets of H_0 at chemical potential $\mu = 0.5$. a_x and a_y are the lattice constants of a unit cell. (b) Phase diagram obtained from solving the linearized gap equation. The blue stars mark the representative points we study for even- and odd-parity pairings in the rest of the Letter. The spatial configurations of the dominant components in the self-consistent solutions with (c) A_g and (d) B_u symmetries, computed on a system with 12 by 12 unit cells. $\Delta_i \equiv |\Delta_{\alpha'\beta'}(\boldsymbol{r}, \boldsymbol{r}')|$ for the bond with the ith largest gap magnitude. $\Delta_{1/2}$ in (c) denotes the magnitude for on-site gaps. A_u and B'_u have similar configurations to that of B_u despite different spin structures.

resulting two electron pockets are centered along the $\Gamma - X$ line [Fig. 2(a)], as observed by ARPES [2].

We consider short-ranged density-density interactions that preserve the lattice symmetries up to nearest-neighbor unit cells [Fig. 1(b)]:

$$H_{\rm int} = \sum_{\boldsymbol{r}\boldsymbol{r}'} \sum_{\alpha\beta\alpha'\beta'} \Gamma_{\alpha'\beta',\beta\alpha}(\boldsymbol{r},\boldsymbol{r}') c^\dagger_{\boldsymbol{r}\alpha'} c^\dagger_{\boldsymbol{r}'\beta'} c_{\boldsymbol{r}'\beta} c_{\boldsymbol{r}\alpha}$$
$$= \sum_{\boldsymbol{r}} U^l n_{\uparrow\sigma l}(\boldsymbol{r}) n_{\downarrow\sigma l}(\boldsymbol{r}) + V_a^{ll'} n_{\sigma l}(\boldsymbol{r}) n_{\sigma' l'}(\boldsymbol{r}+\boldsymbol{\delta}_a), \quad (2)$$

where $\sigma^{(\prime)}$, $l^{(\prime)}$, and $a = 1, 2$ indices are summed over, $n_{s\sigma l}(\boldsymbol{r})$ is the density with spin s and orbital l locating at sublattice σ in the unit cell centered at $\boldsymbol{r}$, and $n_{\sigma l}(\boldsymbol{r}) = \sum_s n_{s\sigma l}(\boldsymbol{r})$. Here U^l denotes the on-site interactions for orbital l, $V_1^{ll'}$ and $V_2^{ll'}$ denote the nearest- and next-nearest-neighbor interactions, respectively, on the zigzag chains with intraorbital (interorbital) characters for $l' = l(\bar{l})$ [Fig. 1(b)], and $\boldsymbol{\delta}_a$ denotes corresponding lattice vectors (SM Sec. I). For simplicity, in the following we consider the case where $U^l = U$, and $V_1^{ll'} = V_2^{ll'} = V$.

Method and phase diagram.—To analyze the dominant pairing channel for given interactions U and V, we first classify the symmetries of possible pairing gaps. The normal state preserves two nonsymmorphic symmetries $C_{2x} = e^{ik_x a_x/2}(-i\hat{s}_x \otimes \hat{\sigma}_x \otimes \hat{l}_0)$, $k_y \to -k_y$, and $M_x = e^{ik_x a_x/2}(-i\hat{s}_x \otimes \hat{\sigma}_0 \otimes \hat{l}_z)$, $k_x \to -k_x$. The mean-field Bogoliubov-de Gennes (BdG) Hamiltonian

$$H^{\rm BdG}_{\boldsymbol{k}} = \begin{bmatrix} H_0(\boldsymbol{k}) & \Delta(\boldsymbol{k}) \\ \Delta^\dagger(\boldsymbol{k}) & -T^\dagger H_0^\dagger(\boldsymbol{k}) T \end{bmatrix} \quad (3)$$

therefore obeys $g^{BdG}_{\boldsymbol{k}} H^{\rm BdG}_{\boldsymbol{k}} (g^{BdG}_{\boldsymbol{k}})^\dagger = H^{\rm BdG}_{g\boldsymbol{k}}$, where $T = is_y\mathcal{K}$, $\boldsymbol{k} \to -\boldsymbol{k}$ is the time-reversal operation with $\mathcal{K}$ the complex conjugation, and $g^{BdG}_{\boldsymbol{k}} = {\rm diag}[g_{\boldsymbol{k}}, \eta_g g_{\boldsymbol{k}}]$ describes how the two symmetries $g = C_{2x}, M_x$ act on the Nambu basis $[c_{\boldsymbol{k}\uparrow}, c_{\boldsymbol{k}\downarrow}, c^\dagger_{\boldsymbol{k}\downarrow}, -c^\dagger_{\boldsymbol{k}\uparrow}]$. Thus, the pairing gaps transform as $g_{\boldsymbol{k}} \Delta_{\boldsymbol{k}} g_{\boldsymbol{k}}^\dagger = \eta_g \Delta_{\boldsymbol{k}}$, and we can classify all possible pairing gaps into four irreducible representations A_g, B_g, A_u, and B_u according to their parities $\eta_g = \pm 1$ under the symmetry transformations g (see Table I).

Next, we determine which irreducible representation has the highest T_c by solving the linearized gap equation [57]

TABLE I. The parities of the irreducible representations under the $1T'$ lattice symmetry operations. The action of the symmetries on crystal momentum and internal indices and the used Nambu basis are shown in the text.

	$\eta_{C_{2x}}$	η_{M_x}	Examples
A_g	+	+	$\hat{s}_0 \otimes \hat{\sigma}_0 \otimes \hat{l}_0$
B_g	−	−	$\hat{s}_0 \otimes \hat{\sigma}_z \otimes \hat{l}_x$
A_u	+	−	$k_x \hat{s}_x \otimes \hat{\sigma}_0 \otimes \hat{l}_z$
B_u	−	+	$k_x \hat{s}_z \otimes \hat{\sigma}_0 \otimes \hat{l}_z$

$\Delta_{\alpha'\beta'}(\boldsymbol{k}') = -\sum_{\boldsymbol{k}''\boldsymbol{k}} \Gamma_{\alpha'\beta',\beta''\alpha''}(\boldsymbol{k}',\boldsymbol{k}'') \times \chi_{\beta''\alpha'',\alpha\beta}(\boldsymbol{k}'',\boldsymbol{k},T) \Delta_{\alpha\beta}(\boldsymbol{k})$, where Greek indices contain all the internal indices (s,σ,l), and repeated indices are summed over. Here, the interaction $\Gamma_{\alpha'\beta',\beta\alpha}(\boldsymbol{k}',\boldsymbol{k})$ is the Fourier transform of $\Gamma_{\alpha'\beta',\beta\alpha}(\boldsymbol{r},\boldsymbol{r}')$ in Eq. (2), and $\chi_{\beta''\alpha'',\alpha\beta}(\boldsymbol{k}'',\boldsymbol{k},T)$ is the noninteracting static pairing susceptibility at temperature T. Solving the linearized gap equation amounts to solving the eigenvalue problem of the effective interaction projected onto the Fermi surface $\tilde{\Gamma}(\boldsymbol{p}',\boldsymbol{p}) = -\sqrt{P_{\boldsymbol{p}'}}\Gamma(\boldsymbol{p}',\boldsymbol{p})\sqrt{P_{\boldsymbol{p}}}$, where $\boldsymbol{p}^{(\prime)}$ is the incoming (outgoing) momentum on the Fermi surface, and $P_{\boldsymbol{p}} = (\sum_{n=1,2} |\boldsymbol{p},n\rangle\langle\boldsymbol{p},n|) \otimes (\sum_{n=1,2} |-\boldsymbol{p},n\rangle\langle-\boldsymbol{p},n|)$ projects an electron-pair state to the two degenerate noninteracting bands n on the Fermi surface at momenta $\boldsymbol{p}$ and $-\boldsymbol{p}$. The eigenvector $\psi(\boldsymbol{p})$ of $\tilde{V}$ with the most negative eigenvalue λ is the solution to the linearized gap equation with the highest $T_c \propto \exp(-1/|\lambda|)$. We can then determine how $\psi(\boldsymbol{p})$ behaves under symmetries C_{2x} and M_x under different interactions and obtain the superconducting phase diagram of $H = H_0 + H_{\rm int}$.

In Fig. 2(b), we present this phase diagram as a function of U and V. We find that while on-site attractions favor the even-parity "trivial" representation A_g as expected, the odd-parity representations A_u and $B_u^{(\prime)}$ (the superscript denotes different pair spin textures) dominate over a large portion of the phase diagram where the nearest-neighbor attraction V dominates. In particular, the degenerate A_u and B_u' gaps at repulsive U are equal-spin triplets in the out-of-plane direction ($|\uparrow\uparrow \mp \downarrow\downarrow\rangle$), and the B_u gap at attractive U has $s_z = 0$ ($|\uparrow\downarrow + \downarrow\uparrow\rangle$). This $SU(2)$-symmetry breaking is due to the intrinsic spin-orbit coupling $V_{\rm soc}$.

We can understand qualitatively the competition between even- and odd-parity pairings from their real-space gap structures. To this end, we write down the mean-field Hamiltonian in Eq. (3) in real space and solve the self-consistency equations $\Delta_{\alpha'\beta'}(\boldsymbol{r},\boldsymbol{r}') = -\sum_{\alpha\beta} \Gamma_{\alpha'\beta',\beta\alpha}(\boldsymbol{r},\boldsymbol{r}') \langle c_{\boldsymbol{r}'\beta} c_{\boldsymbol{r}\alpha}\rangle$ by iteration. We consider the short-ranged interactions $H_{\rm int}$ and show results for representative points for even- and odd-parity pairings [see blue stars in Fig. 2(b)]. We find the dominant component in the even-parity A_g gap to be the on-site pairings as expected, while the dominant contribution to the odd-parity B_u gap comes from the next-nearest-neighbor d-orbital pairing along the chains in the $\hat{\mathbf{x}}$ direction [see the bonds with Δ_1 in Fig. 2(c),(d)]. It is then clear that attractions U^d and V_2^{dd} in Eq. (2) are the main terms responsible for A_g and B_u pairings, respectively. While on-site attractions U^d are uniform in momentum space and promote even-parity pairing, attractive V_2^{dd} terms enhance scattering processes with large momentum-transfer $2k_F$ across the two pockets, which promotes odd-parity pairing (SM Sec. II); hence, the balance between even- and odd-parity pairings as shown in the phase diagram.

Corner Majoranas in WTe_2.—To understand the topological properties of these phases, we examine the boundary modes of different paired states in the phase diagram.

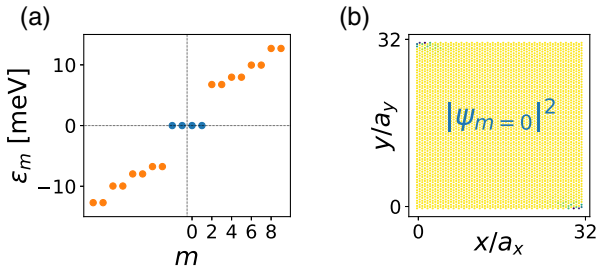

FIG. 3. BdG spectrum for gated WTe_2 with B_u pairing symmetry at $U = -0.2$, $V = -0.4$ on a finite lattice of 32×32 unit cells computed by Lanczos techniques. (a) The gapped BdG spectrum with a near-zero energy Majorana Kramers doublet. (b) The spatial probability distribution $|\psi_0|^2$ corresponding to the zero modes, demonstrating sharp corner localization. The geometry preserves inversion but not the two nonsymmorphic symmetries.

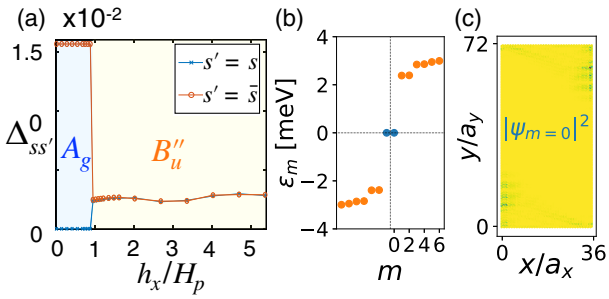

FIG. 4. (a) The evolution of pairing symmetries and dominant order-parameter magnitudes of different spin components Δ^0_{ss} and $\Delta^0_{s\bar{s}}$ when applying an in-plane field with strength h_x to the A_g phase. We consider a representative point $(U, V) = (-1, -0.4)$ [the lower blue star in Fig. 2(b)] and solve the gap equations self-consistently with term $H_{\text{field}} = h_x \hat{s}_x \otimes \hat{\sigma}_0 \otimes \hat{l}_0$ added to Eq. (1). The blue and yellow background colors represent phase A_g and B''_u. For A_g, the opposite-spin component results from spin-singlet pairing. For B''_u, the opposite- and equal-spin components result from spin-triplet states $|\uparrow\downarrow + \downarrow\uparrow\rangle$ and $|\uparrow\uparrow + \downarrow\downarrow\rangle$, respectively. (b) The gapped BdG spectrum with zero-energy modes, and (c) the probability distribution of the zero-energy eigenstate $|\psi_0|^2$ at $h_x/H_p \sim 5.3$.

While the spin-singlet A_g phase is topologically trivial as expected, we find that spin-triplet phases exhibit exotic boundary modes. Specifically, in our model for superconducting WTe_2 given by H_0 and the self-consistently obtained B_u pairing [58], we numerically demonstrate the existence of zero-energy corner-localized states on an open-boundary geometry (Fig. 3). We further verify that with an increasing system size L, these corner states tend exponentially toward zero energy (SM Sec. III), which unambiguously demonstrate the existence of Majorana Kramers pairs localized at two opposite corners. We also find similar Majorana corner modes in the other spin-triplet phase A_u (SM Sec. III).

Even if the realistic WTe_2 lies in the even-parity pairing A_g regime in Fig. 2(b), we find that an intermediate in-plane magnetic field can surprisingly drive a first-order phase transition and stabilize a new equal-spin phase B''_u [59] aligning with the applied field near the Pauli limit [Fig. 4(a)]. This is consistent with the in-plane critical field exceeding the Pauli limit reported by recent experiments [20,21]. Importantly, this field-induced B''_u phase also exhibits two Majoranas localized near opposite corners [Fig. 4(b), (c)]. Due to the broken time-reversal symmetry, these two corner modes are single Majoranas instead of Majorana Kramers pairs (SM Sec. III). We therefore emphasize that even if the superconductivity in the realistic WTe_2 belongs to the even-parity A_g representation, it is still possible to obtain single Majorana corner modes by applying an in-plane field.

A recipe for 2D higher-order superconductors.—We point out that these 2D higher-order superconducting phases can in fact be achieved by a general recipe [60]. Our studies on WTe_2 suggests that corner Majoranas might occur generically from the combination of a gated QSH state with odd-parity superconductivity. This recipe is most intuitive from the boundary perspective. Consider such a QSH normal state at a doping level where it still exhibits counterpropagating modes well-localized on the edge. In the absence of pairing, the corresponding BdG Hamiltonian has two electron-like and two hole-like zero-energy eigenstates with edge-localized wave functions. When we introduce an odd-parity pairing potential, which changes sign in real space when projected onto opposite edges and inevitably vanishes at the domain walls, the electron- and hole-like edge states will mix and acquire finite energies *except* at the two inversion-related points where the projected pairing vanishes. The resulting "leftover" zero-energy modes, whose point-like wave functions will likely to be trapped at corners for realistic samples, therefore lead to two Majorana Kramers pairs localized on two opposite corners. Although the bulk-boundary correspondence is not rigorously proven, we analytically show that corner Majoranas naturally exist in a minimal model we construct for superconductors built from our recipe (SM Sec. VII).

Bulk invariant perspective of the recipe.—This 2D higher-order topological superconducting state is in fact a type of TCsc protected by inversion symmetry. Based on studies of various symmetry-protected topological phases [35,37,61], we conjecture that the bulk topology in inversion-protected TCsc could be inferred from the inversion eigenvalues of occupied BdG bands at TRIMs. With these BdG parity data, we define a symmetry indicator as the bulk invariant for a 2D inversion-protected TCsc in the presence of time-reversal symmetry,

$$\kappa = \frac{1}{4} \sum_{k \in \text{TRIM}} \sum_{n} \xi_{kn}, \tag{4}$$

inspired by indicators proposed for 3D systems [35,37]. Here $\xi_{k,n}$ are the parity eigenvalues of the occupied BdG

bands at TRIMs $\boldsymbol{k}$ [61], and this indicator is stable to adding trivial normal bands for restricted cases where the normal state is half-filled. Application of this formula thus requires extending the "normal" inversion operator I_0 to Nambu space. For odd-parity superconductors, which are defined by superconducting gaps satisfying $I_0\Delta_{\boldsymbol{k}}I_0^{-1} = -\Delta_{\boldsymbol{k}}$, the operator $I = \mathrm{diag}(I_0, -I_0)$ defines the inversion operation for BdG Hamiltonians. For even-parity superconductors, this inversion operator I has no minus sign in the hole part, so κ is always zero [37]. By identifying trivial BdG parity data as those from "atomic superconductors," which are constructed by placing zero-dimensional electron- or hole-like bogoliubons at Wycoff positions, we can see that our indicator is stable upon mod 4. This indicates that the classification of 2D inversion-protected TCsc is Z_4.

To identify which of the four states features corner Majoranas, we relate our index κ to the well-known Z_2 index ν for 2D time-reversal superconductors (SM Sec. IV):

$$\nu = \kappa \mod 2. \tag{5}$$

It is thus clear that $\kappa = 0$, 2 phases do not have edge Majoranas while $\kappa = 1$, 3 phases do. Nonetheless, the $\kappa = 2$ phase is topologically distinct from the trivial $\kappa = 0$ phase, hinting that the former has corner Majoranas.

In fact, the phases hosting corner Majoranas in WTe_2 have $\kappa = 2$, which we explicitly verified using H^{BdG} with self-consistently obtained Δ in Fig. 2(d) (SM Sec. V). Not only for this particular example, here we show that general 2D higher-order superconductors constructed from our recipe have $\kappa = 2$. To see this, we relate the Z_4 indicator κ for a time-reversal parity-odd BdG system to the Z_2 topological index ν_N [62] for its normal state:

$$\kappa = 2\kappa_N, \qquad \nu_N = \kappa_N. \tag{6}$$

Here, $\kappa_N = 0$, 1 is the Z_2 indicator defined analogously as in Eq. (4) but for normal-state Hamiltonians [37]. Importantly, the latter relation holds for a metallic state only when the numbers of occupied bands are all the same at all TRIMs (SM Sec. VI). Now, we follow our recipe and take the normal state to be a gated QSH state whose Fermi surface does not circle any TRIM, just as gated WTe_2. In this case, Eq. (6) holds, and we have $\kappa_N = \nu_N = 1$. Upon introducing odd-parity pairing, the resulting superconductor therefore has $\kappa = 2$.

Discussion.—For the odd-parity paired states we find in WTe_2, which we find to be inversion-protected higher-order TCsc, we expect that the Majorana corner modes cannot be removed without closing the bulk gap if inversion is preserved. When the inversion symmetry is broken, while the Majoranas are no longer protected by the 2D bulk topology, they are still protected by the gaps on the 1D edges. In this case, the paired state becomes the so-called "extrinsic" higher-order topological superconductor [63]. We thus expect these Majorana corner modes can in principle be probed by STM or transport measurements.

This work is supported by Microsoft and Laboratory for Physical Sciences. R.-X. Z. is supported by a JQI Postdoctoral Fellowship. J. S. was supported by the NSF-DMR1555135 (CAREER). The authors acknowledge the University of Maryland supercomputing resources [64] made available for conducting the research reported in this Letter. This research was supported in part (through helpful discussions at KITP) by the National Science Foundation under Grant No. NSF PHY-1748958.

Note added.—After posting this work, we became aware of Ref. [65], which mainly discussed the formulation of symmetry indicators for inversion-protected TCsc in any d dimension. Their $d = 2$ case agrees with our conjecture in Eq. (4) for the cases we focus on.

*yhsu2@nd.edu

[1] X. Qian, J. Liu, L. Fu, and J. Li, Science **346**, 1344 (2014).
[2] S. Tang *et al.*, Nat. Phys. **13**, 683 (2017).
[3] Z. Fei, T. Palomaki, S. Wu, W. Zhao, X. Cai, B. Sun, P. Nguyen, J. Finney, X. Xu, and D. H. Cobden, Nat. Phys. **13**, 677 (2017).
[4] S. Wu, V. Fatemi, Q. D. Gibson, K. Watanabe, T. Taniguchi, R. J. Cava, and P. Jarillo-Herrero, Science **359**, 76 (2018).
[5] P. Li, Y. Wen, X. He, Q. Zhang, C. Xia, Z.-M. Yu, S. A. Yang, Z. Zhu, H. N. Alshareef, and X.-X. Zhang, Nat. Commun. **8**, 2150 (2017).
[6] K. Deng, G. Wan, P. Deng, K. Zhang, S. Ding, E. Wang, M. Yan, H. Huang, H. Zhang, Z. Xu, J. Denlinger, A. Fedorov, H. Yang, W. Duan, H. Yao, Y. Wu, S. Fan, H. Zhang, X. Chen, and S. Zhou, Nat. Phys. **12**, 1105 (2016).
[7] A. H. Castro Neto, Phys. Rev. Lett. **86**, 4382 (2001).
[8] J. A. Wilson, F. J. Di Salvo, and S. Mahajan, Phys. Rev. Lett. **32**, 882 (1974).
[9] J. A. Wilson, F. J. D. Salvo, and S. Mahajan, Adv. Phys. **50**, 1171 (2001).
[10] B. Sipos, A. F. Kusmartseva, A. Akrap, H. Berger, L. Forr, and E. Tuti, Nat. Mater. **7**, 960 (2008).
[11] X. Xi, L. Zhao, Z. Wang, H. Berger, L. Forr, J. Shan, and K. F. Mak, Nat. Nanotechnol. **10**, 765 (2015).
[12] T. Ritschel, J. Trinckauf, K. Koepernik, B. Bchner, M. v. Zimmermann, H. Berger, Y. I. Joe, P. Abbamonte, and J. Geck, Nat. Phys. **11**, 328 (2015).
[13] L. J. Li, E. C. T. OFarrell, K. P. Loh, G. Eda, B. zyilmaz, and A. H. Castro Neto, Nature (London) **529**, 185 (2015).
[14] N. F. Q. Yuan, K. F. Mak, and K. T. Law, Phys. Rev. Lett. **113**, 097001 (2014).
[15] Y.-T. Hsu, A. Vaezi, M. H. Fischer, and E.-A. Kim, Nat. Commun. **8**, 14985 (2017).
[16] J. T. Ye, Y. J. Zhang, R. Akashi, M. S. Bahramy, R. Arita, and Y. Iwasa, Science **338**, 1193 (2012).
[17] J. M. Lu, O. Zheliuk, I. Leermakers, N. F. Q. Yuan, U. Zeitler, K. T. Law, and J. T. Ye, Science **350**, 1353 (2015).

[18] W. Shi, J. Ye, Y. Zhang, R. Suzuki, M. Yoshida, J. Miyazaki, N. Inoue, Y. Saito, and Y. Iwasa, Sci. Rep. **5**, 12534 (2015).
[19] X. Xi, Z. Wang, W. Zhao, J.-H. Park, K. T. Law, H. Berger, L. Forr, J. Shan, and K. F. Mak, Nat. Phys. **12**, 139 (2015).
[20] E. Sajadi, T. Palomaki, Z. Fei, W. Zhao, P. Bement, C. Olsen, S. Luescher, X. Xu, J. A. Folk, and D. H. Cobden, Science **362**, 922 (2018).
[21] V. Fatemi, S. Wu, Y. Cao, L. Bretheau, Q. D. Gibson, K. Watanabe, T. Taniguchi, R. J. Cava, and P. Jarillo-Herrero, Science **362**, 926 (2018).
[22] A. F. Kusmartseva, B. Sipos, H. Berger, L. Forró, and E. Tutiš, Phys. Rev. Lett. **103**, 236401 (2009).
[23] D. Kang, Y. Zhou, W. Yi, C. Yang, J. Guo, Y. Shi, S. Zhang, Z. Wang, C. Zhang, S. Jiang, A. Li, K. Yang, Q. Wu, G. Zhang, L. Sun, and Z. Zhao, Nat. Commun. **6**, 7804 (2015).
[24] X.-C. Pan, X. Chen, H. Liu, Y. Feng, Z. Wei, Y. Zhou, Z. Chi, L. Pi, F. Yen, F. Song, X. Wan, Z. Yang, B. Wang, G. Wang, and Y. Zhang, Nat. Commun. **6**, 7805 (2015).
[25] Z. Chi, X. Chen, F. Yen, F. Peng, Y. Zhou, J. Zhu, Y. Zhang, X. Liu, C. Lin, S. Chu, Y. Li, J. Zhao, T. Kagayama, Y. Ma, and Z. Yang, Phys. Rev. Lett. **120**, 037002 (2018).
[26] Y. Yu, F. Yang, X. F. Lu, Y. J. Yan, Y.-H. Cho, L. Ma, X. Niu, S. Kim, Y.-W. Son, D. Feng, S. Li, S.-W. Cheong, X. H. Chen, and Y. Zhang, Nat. Nanotechnol. **10**, 270 (2015).
[27] F. Wu, T. Lovorn, E. Tutuc, and A. H. MacDonald, Phys. Rev. Lett. **121**, 026402 (2018).
[28] F. Wu, T. Lovorn, E. Tutuc, I. Martin, and A. H. MacDonald, Phys. Rev. Lett. **122**, 086402 (2019).
[29] Z.-Y. Jia, Y.-H. Song, X.-B. Li, K. Ran, P. Lu, H.-J. Zheng, X.-Y. Zhu, Z.-Q. Shi, J. Sun, J. Wen, D. Xing, and S.-C. Li, Phys. Rev. B **96**, 041108(R) (2017).
[30] L. Peng, Y. Yuan, G. Li, X. Yang, J.-J. Xian, C.-J. Yi, Y.-G. Shi, and Y.-S. Fu, Nat. Commun. **8**, 659 (2017).
[31] C. L. Kane and E. J. Mele, Phys. Rev. Lett. **95**, 226801 (2005).
[32] B. A. Bernevig and S.-C. Zhang, Phys. Rev. Lett. **96**, 106802 (2006).
[33] X.-L. Qi, T. L. Hughes, and S.-C. Zhang, Phys. Rev. B **81**, 134508 (2010).
[34] F. Zhang, C. L. Kane, and E. J. Mele, Phys. Rev. Lett. **111**, 056402 (2013).
[35] E. Khalaf, H. C. Po, A. Vishwanath, and H. Watanabe, Phys. Rev. X **8**, 031070 (2018).
[36] E. Khalaf, Phys. Rev. B **97**, 205136 (2018).
[37] S. Ono, Y. Yanase, and H. Watanabe, Phys. Rev. Research **1**, 013012 (2019).
[38] W. A. Benalcazar, B. A. Bernevig, and T. L. Hughes, Science **357**, 61 (2017).
[39] Q. Wang, C.-C. Liu, Y.-M. Lu, and F. Zhang, Phys. Rev. Lett. **121**, 186801 (2018).
[40] Z. Yan, F. Song, and Z. Wang, Phys. Rev. Lett. **121**, 096803 (2018).
[41] Y. Wang, M. Lin, and T. L. Hughes, Phys. Rev. B **98**, 165144 (2018).
[42] F. Schindler, A. M. Cook, M. G. Vergniory, Z. Wang, S. S. P. Parkin, B. A. Bernevig, and T. Neupert, Sci. Adv. **4**, eaat0346 (2018).
[43] J. Langbehn, Y. Peng, L. Trifunovic, F. von Oppen, and P. W. Brouwer, Phys. Rev. Lett. **119**, 246401 (2017).
[44] H. Shapourian, Y. Wang, and S. Ryu, Phys. Rev. B **97**, 094508 (2018).
[45] N. Bultinck, B. A. Bernevig, and M. P. Zaletel, Phys. Rev. B **99**, 125149 (2019).
[46] Y. Xu, Z. Song, Z. Wang, H. Weng, and X. Dai, Phys. Rev. Lett. **122**, 256402 (2019).
[47] R.-X. Zhang, W. S. Cole, and S. Das Sarma, Phys. Rev. Lett. **122**, 187001 (2019).
[48] R.-X. Zhang, W. S. Cole, X. Wu, and S. Das Sarma, Phys. Rev. Lett. **123**, 167001 (2019).
[49] F. Zheng, C. Cai, S. Ge, X. Zhang, X. Liu, H. Lu, Y. Zhang, J. Qiu, T. Taniguchi, K. Watanabe, S. Jia, J. Qi, J.-H. Chen, D. Sun, and J. Feng, Adv. Mater. **28**, 4845 (2016).
[50] R. A. Klemm, A. Luther, and M. R. Beasley, Phys. Rev. B **12**, 877 (1975).
[51] M_x can be transformed back to the conventional mirror symmetry by shifting the mirror plane away from inversion center.
[52] L. Muechler, A. Alexandradinata, T. Neupert, and R. Car, Phys. Rev. X **6**, 041069 (2016).
[53] S. Ok, L. Muechler, D. Di Sante, G. Sangiovanni, R. Thomale, and T. Neupert, Phys. Rev. B **99**, 121105 (2019).
[54] Ref. [55]showed that more spin-orbit coupling terms are required for a better fit to the experimental data. We nonetheless expect our results to change only quantitatively.
[55] A. Lau, R. Ray, D. Varjas, and A. Akhmerov, Phys. Rev. Mater. **3**, 054206 (2019).
[56] See Supplemental Material at http://link.aps.org/supplemental/10.1103/PhysRevLett.125.097001 for details about the WTe_2 model and its properties, the proposed symmetry indicator, and a minimal model demonstrating bulk-boundary correspondence.
[57] M. Sigrist, AIP Conf. Proc. **789**, 165 (2005).
[58] For numerical convenience, we take the self-consistent B_u symmetry solution and multiply by 10 so that the resulting superconducting gaps are always much larger than any finite-size gaps of the normal bulk or edge states for tractable lattice sizes.
[59] The superscript denotes a different spin orientation from that of $B_u^{(\prime)}$.
[60] There could be more recipes to achieve such a phase.
[61] L. Fu and C. L. Kane, Phys. Rev. B **76**, 045302 (2007).
[62] C. L. Kane and E. J. Mele, Phys. Rev. Lett. **95**, 146802 (2005).
[63] M. Geier, L. Trifunovic, M. Hoskam, and P. W. Brouwer, Phys. Rev. B **97**, 205135 (2018).
[64] http://hpcc.umd.edu.
[65] A. Skurativska, T. Neupert, and M. H. Fischer, Phys. Rev. Research **2**, 013064 (2020).